Air Quality, Atmosphere & Health (2021) 14:217–233
https://doi.org/10.1007/s11869-020-00927-2

Inactivation times from 290 to 315 nm UVB in sunlight for SARS coronaviruses CoV and CoV-2 using OMI satellite data for the sunlit Earth

Jay Herman[1] · Bryan Biegel[2] · Liang Huang[3]

Received: 27 June 2020 / Accepted: 30 August 2020 / Published online: 15 September 2020

Abstract

UVB in sunlight, 290–315 nm, can inactivate SARS CoV and SARS CoV-2 viruses on surfaces and in the air. Laboratory exposure to ultraviolet irradiance in the UVC range inactivates many viruses and bacteria in times less than 30 min. Estimated UVB inactivation doses from sunlight in J/m^2 are obtained from UVC measurements and radiative transfer calculations, weighted by a virus inactivation action spectrum, using OMI satellite atmospheric data for ozone, clouds, and aerosols. For SARS CoV, using an assumed UVC dose near the mid-range of measured values, D_{90} = 40 J/m^2, 90% inactivation times T_{90} are estimated for exposure to midday 10:00–14:00 direct plus diffuse sunlight and for nearby locations in the shade (diffuse UVB only). For the assumed D_{90} = 40 J/m^2 model applicable to SARS CoV viruses, calculated estimates show that near noon 11:00–13:00 clear-sky direct sunlight gives values of T_{90} < 90 min for mid-latitude sites between March and September and less than 60 min for many equatorial sites for 12 months of the year. Recent direct measurements of UVB sunlight inactivation of the SARS CoV-2 virus that causes COVID-19 show shorter T_{90} inactivation times less than 10 min depending on latitude, season, and hour. The equivalent UVC 254 nm D_{90} dose for SARS CoV-2 is estimated as 3.2 ± 0.7 J/m^2 for viruses on a steel mesh surface and 6.5 ± 1.4 J/m^2 for viruses in a growth medium. For SARS CoV-2 clear-sky T_{90} on a surface ranges from 4 min in the equatorial zone to less than 30 min in a geographic area forming a near circle with solar zenith angle < 60^O centered on the subsolar point for local solar times from 09:00 to 15:00 h.

Keywords COVID-19 · SARS CoV · Inactivation · Radiative transfer · Ozone · UVB · UVC

Introduction

Onset of coronavirus induced diseases (e.g., 2002, severe acute respiratory syndrome, SARS, (virus, SARS-CoV), 10 years later Middle East respiratory syndrome MERS (virus, MERS-CoV), and starting in 2019, a new viral mutation, SARS-CoV-2, causing COVID-19, has promoted increased interest in methods of deactivating the virus on surfaces through chemical biocidal agents (Kampf et al. 2020) or UVGI (ultraviolet germicidal irradiation) (Anderson et al. 2013; Bedell et al. 2016; Heßling et al. 2020; Lytle and Sagripanti 2005; Sagripanti and Lytle 2020; Kowalski et al. 2009; Kowalski 2009). Most of the work on effective UVGI was performed with radiation in the UV-C range (100–280 nm), usually from low pressure mercury lamps at 254 nm. Sunlight reaching the Earth's surface does not contain significant irradiance for wavelengths less than 290 nm because of absorption by atmospheric ozone and increased Rayleigh scattering with decreasing wavelength. However, there is smaller but significant viral inactivation by UVB wavelengths contained in sunlight in the range 290 to 315 nm (Eisenstark 1987; Nelson et al. 2018). Recently, it has been shown directly that UVB in amounts present in summer sunlight can inactivate the SARS-CoV-2 viruses efficiently (Ratnesar-Shumate et al. 2020) when the virus droplets are dried onto stainless-steel mesh (90% in about 10 min) and in growth medium in about 17 min.

Electronic supplementary material The online version of this article (https://doi.org/10.1007/s11869-020-00927-2) contains supplementary material, which is available to authorized users.

✉ Jay Herman
Herman@umbc.edu

[1] University of Maryland Baltimore County JCET, Baltimore, MD, USA

[2] NASA Ames Research Center, Moffett Field, CA, USA

[3] Science Systems and Applications, Lanham, MD, USA

Inactivation sensitivity to 254 nm UVC radiation is frequently measured in terms of the dose D_{90} (J/m_2) needed to reduce the number of active virus particles by 90%. Measurements by Walker and Ko (2007) showed an inactivation of 87.8% aerosolized murine hepatitis coronavirus (MHV) for an exposure to 254 nm UVC of 5.99 J/m^2, which corresponds to D_{90} = 6.6 J/m^2 (Table 1 and Online Resource 1: Figs. S1 to S4). This inactivation dose is similar to that of the Berne virus Coronaviridae (Weiss and Horzinek 1986; Lytle and Sagripanti 2005; Kowalski et al. 2020a, b), which we estimate to be 7.1 J/m^2 (Fig. S2). A measurement by Liu et al. 2003 on the MHV coronavirus in liquid yielded D_{90} = 95 J/m^2 (Fig. S4). While both viruses are in the coronavirus family, their UV inactivation sensitivity may not be representative of either the SARS-CoV or MERS-CoV variants. Inactivation of CoV-P9 by UVC (Duan et al. 2003) showed undetectable amounts of virus after 60 min of irradiation to 0.9 W/m^2, which, in a company report, Kowalski et al. (2020a, b) estimated D_{90} = 40 J/m^2. Evaluation of a laboratory study by Kariwa et al. (2004) on SARS CoV (Hanoi) gives 46 J/m^2 (Fig. S1) and SARS CoV (Urbani) 1826 J/m^2 (Fig. S3) based on laboratory studies by Darnell et al. (2004). Kowalski et al. (2020a, b) obtained different values of D_{90} = 134 J/m^2 and 2410 J/m^2, respectively. https://avdc.gsfc.nasa.gov/pub/DSCOVR/JayHerman/COVID-19/).

A fast calculation method is used (Online Resource 2: Eqns. S2 to S10) for globally estimating the inactivation of SARS CoV by sunlight using satellite data, the action spectrum from Lytle and Sagripanti (2005), and a nominal value of D_{90} = 40 J/m^2 (close to the SARS CoV Hanoi value of 46 J/m^2) to estimate the time for 90% inactivation T_{90} for a large number of cities worldwide (Online Resource 3 Table S1) and the number of months where monthly averages (1 to 12) of T_{90} ≤ 120 min. The T_{90} results are linearly proportional to the assumed value of D_{90}.

Heßling et al. (2020) discuss possible reasons for the large variations in measured D_{90}, items 1 to 6 in Table 1. They also conclude, "The calculated upper limit for the log-reduction median dose (in low-absorbance media) is 10.6 mJ/cm^2, but the probably more precise estimation is 3.7 mJ/cm^2." This corresponds to 106 J/m^2 and 37 J/m^2, respectively, the latter close to the nominal value of 40 J/m^2 assumed here.

Since the Ratnesar-Shumate et al. (2020), (RS) measurements are made using simulated clear-sky sunlight in the 290 to 315 nm range, the fast calculation method based on $A(\lambda)$ for measurements made at 254 nm is not needed for estimating T_{90} as a function of solar UVB irradiance for their measurement conditions. In order to generalize the RS measurements, an estimate of the equivalent 254 nm D_{90} amount is obtained by matching their measurement conditions and results using the TUV radiative transfer calculations. The estimated 254 nm inactivation D_{90} of SARS CoV-2 (Table 1) gives globally distributed estimates of RS T_{90}.

Inactivation calculation by UVGI from sunlight UVB

To estimate the effect of sunlight in the 290 ≤ λ ≤ 315 nm UVB range that reaches the Earth's surface at significant intensity, a transfer function from 254 nm to UVB (290–315 nm), or action spectrum $A(\lambda)$ is needed that is normalized to 1 at 254 nm (Fig. 1 from Lytle and Sagripanti 2005) (Eqs. 1 and 2 and Fig. 1). The analysis is based on an application of TUV (Madronich 1993, 1995) atmospheric radiative transfer calculation using ozone monitoring instrument (OMI) satellite data total column ozone (TCO_3), estimated cloud transmission C_T, and absorbing aerosol transmission C_A to derive a useful formulation for high-speed evaluation (Herman 2010; Herman et al. 2018, 2020). The results are presented in terms of dosage (D) in J/m^2 and inactivation time (T_{90}) in minutes from UV solar radiation to achieve 90% inactivation relative to the D_{90} exposure at 254 nm.

For SARS CoV, estimates of UVB T_{90} are obtained from UVC measurements for 4 open land sites and 190 cities in Europe, North America, South America, Asia, and Australia. Analysis is presented for monthly averages $<T_{90}>$ of clear and cloudy days from 12:00 ± 4 h local solar time and compared to noon virus inactivation times. The goal is to determine how many days of the year the inactivation time from UVB

Table 1 Estimation of UVC D90 (Figs. S1 to S4, items 1-6) and later section for items 7–8

Item	D_{90} (J/m^2)	Data reference
1	7.1	Berne-CV (Weiss and Horzinek 1986).
2	40	CoV-P9 by UVC (Duan et al. 2003; Kowalski et al. 2020a, b)
3	46	SARS CoV (Hanoi) (Kariwa et al. 2004)
4	1826	SARS-CoV (Urbani) (Darnell et al. 2004)
5	95	Murine Hepatitis Coronavirus (MHV) (Liu et al. 2003)
6	6.6	Murine Hepatitis Coronavirus (MHV) Airborne (Walker and Ko 2007)
7	3.2	SARS CoV-2 dried on steel mesh UVC D_{90} estimated
8	6.5	SARS CoV-2 in growth medium UVC D_{90} estimated

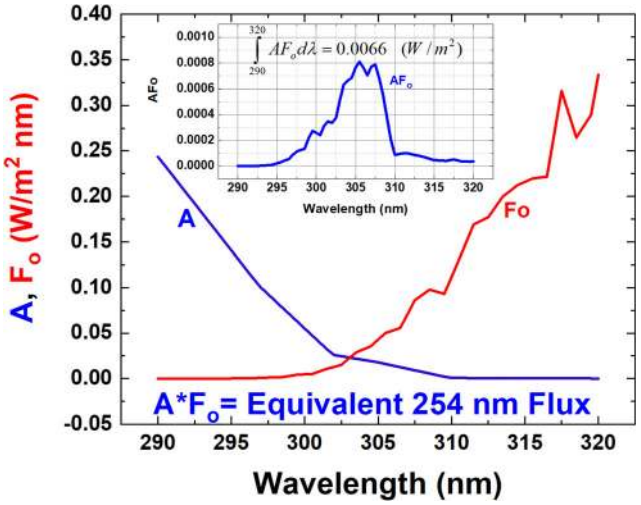

Fig. 1 The viral inactivation spectrum $A(\lambda)$ normalized to 1 at 254 nm (blue), solar irradiance (red) at the Earth's surface F_O(W/m^2 nm), and the product $AF_O(\lambda)$ (inset) for $\theta = 30^O$ and $\Omega = 325$ DU

sunlight was short enough to have a significant impact on decontamination of surfaces and airborne coronaviruses in direct sunlight or in nearby shade. Most of the analysis is based on the assumption that laboratory inactivation data for virus particles suspended in an aqueous solution, which absorbs some of the UVC, applies to surfaces and aerosolized particles suspended in air and that $A(\lambda)$ is valid for coronaviruses. The data in Table 1 suggests that T_{90} for aerosolized virus particle in air or on surfaces is shorter than viruses in liquids. The T_{90} times for both SARS CoV and SARS CoV-2 on surfaces are given as a function of latitude and season using a uniform calculation method for all cases considered.

Key components for estimating T_{90} for a coronavirus are (1) an estimate of the normalized action spectra $A(\lambda)$ representing the relative efficiency for a wavelength λ compared to the much stronger inactivation rate at the UVC wavelength 254 nm; (2) a calculated estimate of the solar irradiance reaching the Earth's surface as a function of solar zenith angle (θ = SZA), total column ozone amount (Ω = TCO_3) over a specified site, fractional cloud transmission C_T of UV irradiance using measured Lambert equivalent reflectivity (LER) of the scene, and fractional absorbing aerosol transmission (C_A), all as a function of latitude ζ, longitude ϕ, altitude z, and day of the year (DOY). The same method is applied for SARS CoV-2 after calculating the equivalent 254 nm D_{90}.

Atmospheric data is obtained from measurements by the OMI onboard the US Aura satellite (2004–present). OMI is a polar orbiting nadir and side viewing satellite instrument (2600-km-wide swath on the surface) providing near global coverage (nadir resolution field of view 13 km × 24 km) once per day from a 90-min polar orbit with an equator crossing time of approximately 13:30 local solar time (LST) (Levelt et al. 2018). For computational purposes, the input data have been averaged onto a $1^O \times 1^O$ latitude × longitude grid https://avdc.gsfc.nasa.gov/pub/tmp/OMI_Daily_O3_and_LER/. OMI data are filtered to remove data from bad detector pixels and for the known so-called row anomaly (Schenkeveld et al. 2017).

Additional data from the Deep Space Climate Observatory (DSCOVR) Earth Polychromatic Imaging Camera (EPIC) in orbit about the Earth-Sun Lagrange-1 point L_1, 1.5 million kilometers from Earth, are used for science products and color pictures of the entire sunlit Earth at specific Greenwich Mean Times (GMT).

The solar irradiance spectrum output (W/m^2 nm) at the Earth's surface $F(\zeta,\phi,\theta,\lambda,\Omega,z)$, calculated from the TUV model, is obtained for $100 \le \Omega \le 600$ Dobson Units (1 DU = 2.687 × 10^{16} molecules/cm^2), for SZA range $0^O \le \theta \le 80^O$, and for an altitude range $0 \le z \le 8$ km. The TUV spectral output is multiplied by a normalized action spectrum $A(\lambda)$ and integrated over the non-zero range of $F(\lambda)A(\lambda)$ (Fig. 1 and Eq. 1).

$$P(\varsigma,\phi,\theta,\Omega,z) = \int_{290}^{320} F(\varsigma,\phi,\theta,\lambda,\Omega,z)A(\lambda)d\lambda \quad (1)$$

The TUV output $P(\theta,\Omega)$ can be used as a table look up or converted to a very accurate functional fit (Online Resource 2: Eqns. S2 to S10), where the latter is much faster for computational purposes. The small error estimates for this type of functional fit are also given (Herman 2010).

The action spectrum $A(\lambda)$ (Lytle and Sagripanti 2005) is approximated by a rational fraction fit for the range $290 \le \lambda \le 320$ nm (Eq. 2 and Table 2):

$$A(\lambda) = \frac{a_1 + a_2\theta^{0.5} + a_3\theta}{1 + b_1\theta^{0.5} + b_2\theta} \quad (2)$$

For a case at $z = 0$ km, $F_O = F(\zeta,\phi,\theta,\lambda,\Omega,0)$, $\Omega = 325$ DU, and $\theta = 30^O$. $P(\zeta,\phi,\theta,\Omega,0) = 0.0066 \pm 0.0013$ W/m^2 as shown in Fig. 1. The 20% uncertainty in P, ± 0.0013, arises from uncorrelated error estimates for $A(\lambda)$. Figure 1 shows clear-sky irradiance at the ground $F_OA(\lambda)$ peaking near 305 nm. While the amount of clear-sky 305 nm solar irradiance at the ground is small compared to longer wavelengths, because of attenuation by ozone and Rayleigh scattering, it is significant for viral inactivation (Fig. 1)

Table 2 Coefficients for A(λ) and see Fig. 1

n	a_n	b_n
1	0.03185621255581713	− 0.1171817797253023
2	− 0.003565593470829207	0.003433857833125471
3	9.976358190920908x10^{-05}	

The next step is translating the atmospheric calculations of $P(\theta,\Omega,0)$ for the Earth's surface at sea level ($z = 0$) into a 90% inactivation time T_{90} as a function of SZA. Laboratory values of the logarithmic decay of viruses of starting number N_O exposed to 254 nm UV light for exposure D (J/m^2) are measured as a function of time to determine the slope k of the decay curve as a function of the survival fraction N/N_O (Eq. 3).

$$N/N_O = e^{-kD} \;\; or \;\; k = -\frac{1}{D} Ln(N/N_O) \tag{3}$$

When $D = D_{90}$ (J/m^2), it is an exposure representing 10% survival, $N/N_O = 0.1$. More complicated two-slope inactivation models have been used when the inactivation vs. D show two log-linear slopes (Kowalski et al. 2020a, b) for inactivation times greater than T_{90}.

Figure 2 expands the calculation for a range of SZA and TCO_3 values from 150 to 400 DU, spanning the range of TCO_3 expected over latitudes from 65^{O}S to 65^{O}N on most days of the year. Average equatorial TCO_3 is smaller than average mid-latitude values and the minimum SZA is smaller so that equatorial T_{90} is shorter than for mid-latitudes.

To obtain the 90% inactivation time T_{90} from the integrated product of $A(\lambda)F_O(\lambda)$ and the measured value of D_{90}, the following formula (Eq. 4) is used:

$$T_{90} = \frac{D_{90}}{60} / \int_{290}^{320} A(\lambda) F_o(\lambda) d\lambda \tag{4}$$

The factor 60 converts the units from seconds to minutes. For SARS CoV, the nominal value D_{90} = 40 J/m^2 is used in the graphs below as a middle value in Table 1 close to the SARS CoV Hanoi value of 46 J/m^2.

For UV irradiance in the vicinity of 305 nm, there is considerable scattered diffuse light caused by strong Rayleigh scattering causing a clear atmosphere in longer wavelengths (Fig. 3a) to appear more like a light fog in short wavelength UVB (Fig. 3b). Surfaces that appear to be in the shade in visible light are bathed in diffuse light (Fig. 3) that is 60% to 70% of the total $A(\lambda)$ weighted irradiance (diffuse + direct) for $\theta < 40^O$ (Fig. 3). T_{90}(diffuse, $\theta < 40^O$) is 1.4 to 1.7 times T_{90}(total, $\theta < 40^O$). Figures 2 and 3 imply that horizontal surfaces permanently left outside and exposed to midday solar UVB irradiances will have coronaviruses 90% inactivated in less than 120 min for mid- or low-latitude sites for D_{90} = 40 J/m^2. For the UVB inactivation measurements on SARS CoV-2 (Ratnesar-Shumate et al. 2020), T_{90} values in Fig. 2 are reduced by a factor of 12.5 (for SZA = 0^o, 6 min TCO_3 = 375DU, 5 min TCO_3 = 325 DU, 3.5 min TCO_3 = 275 DU) .

For airborne virus particles the actinic flux or fluence is of interest, which is the sum of the upward and downward irradiance, increasing the total UVB exposure by about 5% near the surface of the Earth relative to the total downward irradiance. There is evidence that aerosolized airborne virus particles are more susceptible to UVC than samples measured in liquid (Table 1).

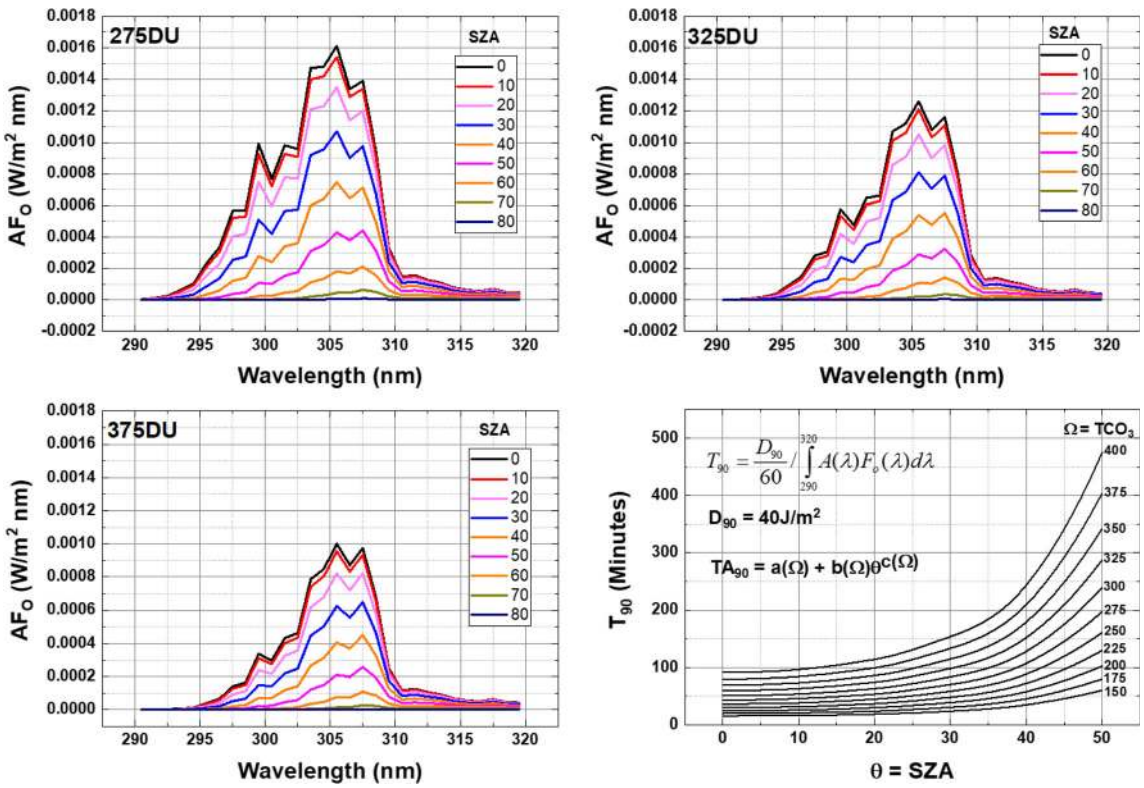

Fig. 2 A sample calculation of AFO for clear-sky conditions for Ω = 150 - 400 DU, and the 90% inactivation time T_{90} as a function of SZA using Eqs. 1, 2, and 4. TA_{90} is a polynomial approximate fit to T_{90}

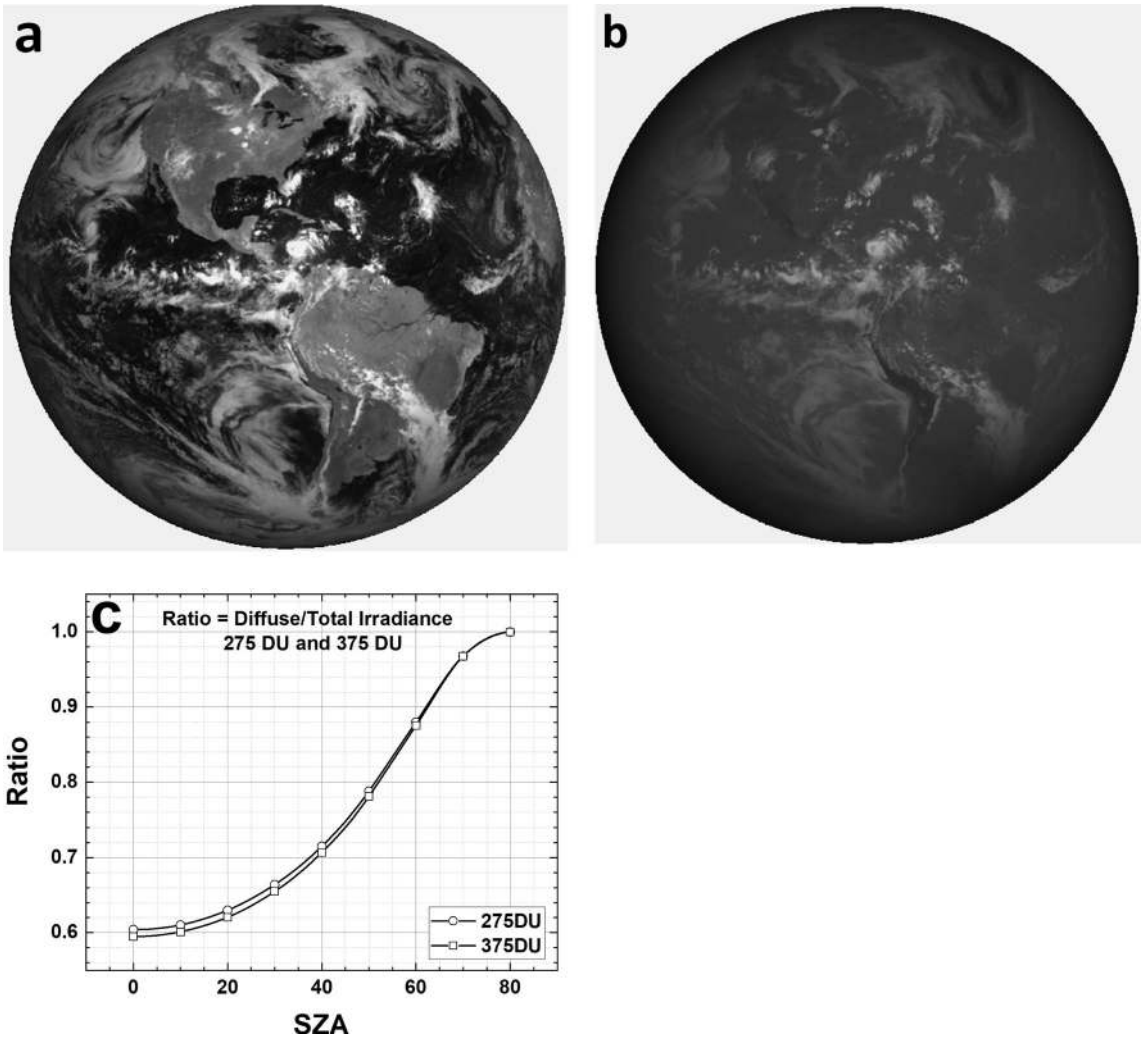

Fig. 3 **a** The Earth as viewed by DSCOVR EPIC at 317 nm showing the effect of Rayleigh scattering. **b** the same scene but at 780 nm. **c** the calculated ratio of $P(\lambda)$ diffuse divided by diffuse plus direct sunlight as a function of SZA for TCO_3 = 275 DU and 375 DU

Estimation of T_{90} from satellite data

To efficiently expand the calculation of T_{90} to use satellite data on a global basis for daily calculations as a function of latitude and longitude, an efficient representation (Eq. 5) is needed for the calculated irradiances from the TUV radiative transfer calculation over the $\theta \times \Omega \times z$ space for the Earth at 1 astronomical unit AU distance from the sun. An allometric form (Eq. 5) accurately fits the TUV output from (Eq .1) for a wide range of θ and Ω (Herman 2010), and altitude z, where $U(\theta)$ and $R(\theta)$ are numerical fitting coefficients defined below (Online Resource 2 and Fig. 4). $R(\theta)$ is an improved version of the radiation amplification factor.

$$P(\theta, \Omega, z, C_T C_A, H, D_S) = U(\theta)\left(\frac{\Omega}{200}\right)^{-R(\theta)} C_T C_A H(z) D_S \quad (5)$$

$$\frac{\partial P}{P} = -R(\theta)\frac{\partial \Omega}{\Omega}$$

Here, the dependence on latitude and longitude (ζ, ϕ) is not explicitly indicated:

C_T cloud transmission fraction between 0 and 1
C_A aerosol transmission fraction between 0 and 1
$H(z)$ topography height factor relative to sea level between 0 and 8 km
D_S correction factor for the distance of the Earth from the sun relative to 1 AU

These quantities are quantitively defined (Online Resource 2: Eqns. S2 to S10, Herman and Celarier 1997; Mok et al. 2018; Torres et al. 2007).

The principal source of error in the radiative transfer calculation method is from uncertainty in the measured ozone value of $\Delta\Omega$ = ± 1 to ± 2%, which would cause an error in in $P_O(\theta,\Omega)$ of $1.7\Delta\Omega$ for low θ and $2.4\Delta\Omega$ for $\theta = 80^O$ (Eq 5, Online Resource 2: Fig. S5). Highly polluted cities will have less irradiance at the ground than estimated from Eq. 5

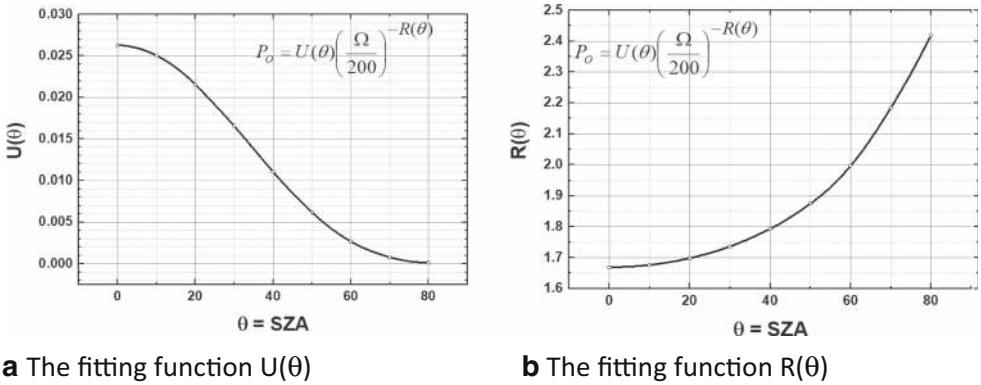

a The fitting function U(θ) **b** The fitting function R(θ)

Fig 4 **a** The fitting function $U(\theta)$ in Eq. 5. **b** The fitting function $R(\theta)$ in Eq. 5

because of the area averaging over the satellite field of view that can include less polluted areas. These errors have been shown to be about 20% calculated overestimation of irradiance at the surface (Lakkala et al. 2020). The accuracy of the TUV calculation compared to ground-based measurements for clear skies has been evaluated (Michalsky and Kiedron 2008) showing an irradiance overestimation for TUV of 1 to 2%. The minimum inactivation times central to this analysis are for days with low reflectivity (little or no clouds) and low aerosol absorption. Errors in the fitting functions are negligible (Herman 2010) by comparison.

Applying the radiative transfer fitting equations to the nearly complete global coverage afforded by OMI's field of view enables $P(\lambda,\theta,\zeta,\phi,z)$ to be determined for any location (ζ, ϕ) as a function of DOY (January 2005 to December 2019). Only the 2019 data are shown. T_{90} is shown for 12 locations representing major cities in the USA, Asia, Australia, Europe, and South America, some strongly affected by COVID-19. A total of 190 cities and 4 land sites are listed (Online Resource 3: Table) showing the 2019 minimum of 12 noontime monthly averages $<T_{90}>$ of daily noontime T_{90} ($_{\text{Min}} <T_{90}>_{12:00}$, columns 4 and 6), and the number of months N_m (columns 5 and 7) in 2019 where noontime $<T_{90}>$ is 120 min or less**.** These averages include the effects of daily cloud and aerosol cover.

For cities at mid-latitudes between 30^O and 40^O (Fig. 5), there is a period where the noontime T_{90} is approximately

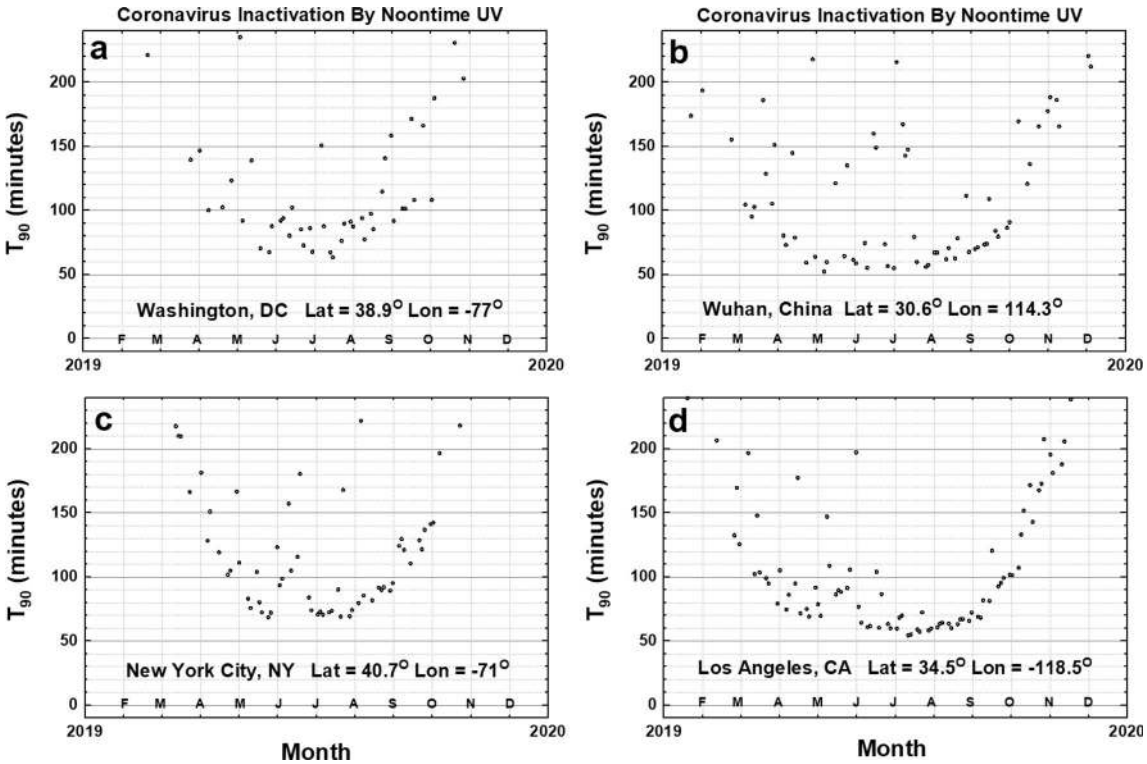

Fig. 5 Noontime T_{90} inactivation times for coronavirus in minutes for Washington DC, US; Wuhan, CN; New York City, US; and Los Angeles, US; and using D_{90} = 40 J/m^2. For the calculated Ratnesar-Shumate et al. (2020) SARS CoV-2 D_{90} = 3.2 J/m^2, T_{90} in June would be about 4.8 for Washington, 4.4 for Wuhan, 5.6 New York City, and 4.8 min for Los Angeles. Figures are truncated at 240 min

60–80 min and lasts for several months. For New York City at 40.7^{O} N, the number of months, T_{90} < 80 min, is less (May to August) than for Los Angeles (April to September). The scatter in the points is mainly due to clouds causing time-varying C_T.

When the D_{90} = 40 J/m^2 calculation is applied to four European cities (Fig. 6) (latitudes 40^{O} to 53^{O}), the periods of 60–80 min inactivation are reduced to where London, England's and Berlin, Germany's shortest T_{90} inactivation times are close to 70–90 min and quickly increase as the local time differs from noon or the month differs from the June solstice (θ increasing). Two other cities, Rome, Italy and Madrid, Spain, have T_{90} values similar to New York City and have minimum T_{90} of 60 to 70 min in June, July, and August.

Figure 7 shows the lack of significant θ dependence for a city in the equatorial zone; Bogota, Colombia at an altitude of 2.5 km with T_{90} = 50 min on many days of the year. The remaining three cities in Fig. 7 are in the Southern Hemisphere, which means their summer period is shifted 6 months with the minima of T_{90} occurring in December and January. T_{90} for Cape Town, South Africa at 39.3^{O} S behaves in a manner similar to New York City at 40.7^{O} N. For the sites shown in Figs. 6 and 7 minimum noontime T_{90} is less than 10 min for the SARS CoV-2 virus with D_{90} = 3.2 J/m^2.

Figure 8 summarizes the 190 city table (Online Resource 3: Table S1). Almost all the equatorial zone cities show 12 months of $<T_{90}>_{12:00} \leq 50$ min. The number of months for $<T_{90}>_{12:00} \leq 120$ min decreases with increasing latitude. In Fig. 8a, the rate of decrease for the Northern Hemisphere (NH) is 3.0 months per 10^{O} and in the Southern Hemisphere (SH) it is 2.6 months per 10^{O} of latitude away from the equatorial zone, although there are fewer points to accurately determine the SH slope.

The equatorial zone shows that most of the minimum values of $_{Min}<T_{90}>_{12:00}$ are less than 50 min (Fig. 8b) up to about ± 25^{O} latitude for sites with fewer cloudy days per month. For latitudes outside the equatorial zone, where both the ozone amounts and SZA are larger, $_{Min}<T_{90}>_{12:00}$ increases. High mountain area sites also have lower noontime minimum $_{Min}<T_{90}>_{12:00}$ than sea-level sites.

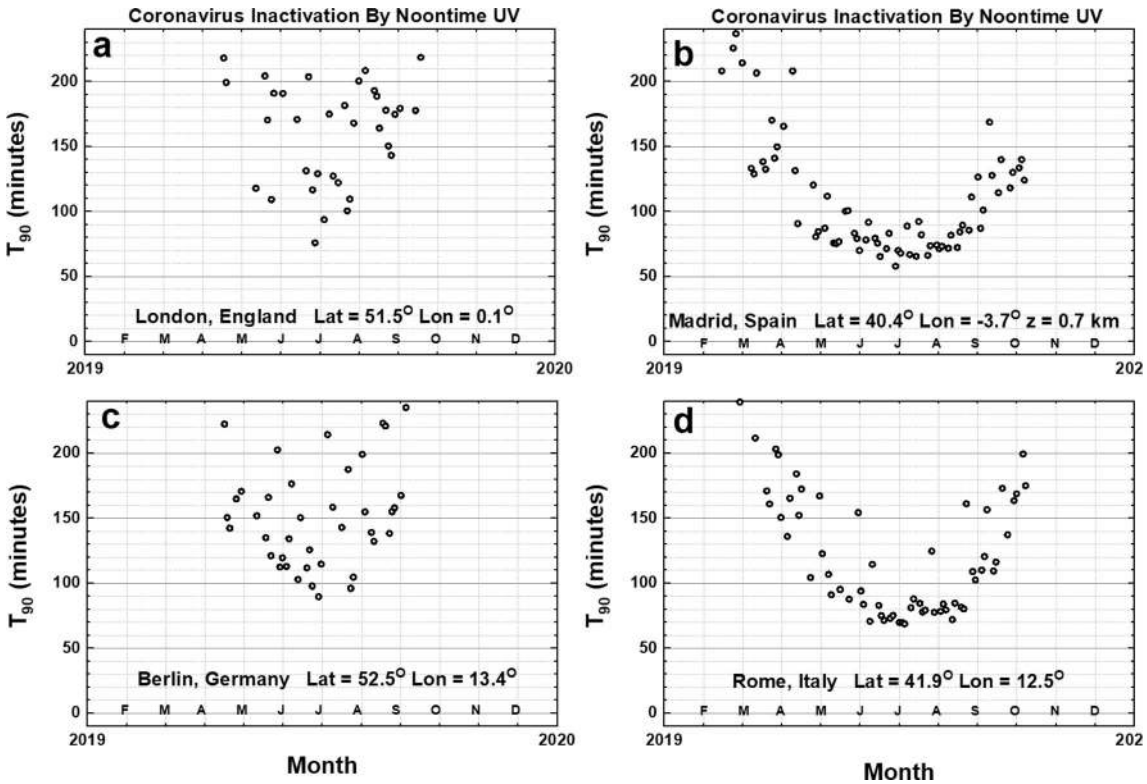

Fig. 6 Noontime T_{90} coronavirus inactivation times for four Cities in Europe, London, UK; Madrid, ES; Berlin, DE; and Rome, IT, using D_{90} = 40 J/m^2. For the calculated RS SARS CoV-2 D_{90} = 3.2 J/m^2, T_{90} in June would about 8 min for London, 5 min for Madrid, 8 min for Berlin, and 5 min for Rome. Figures are truncated at 240 min

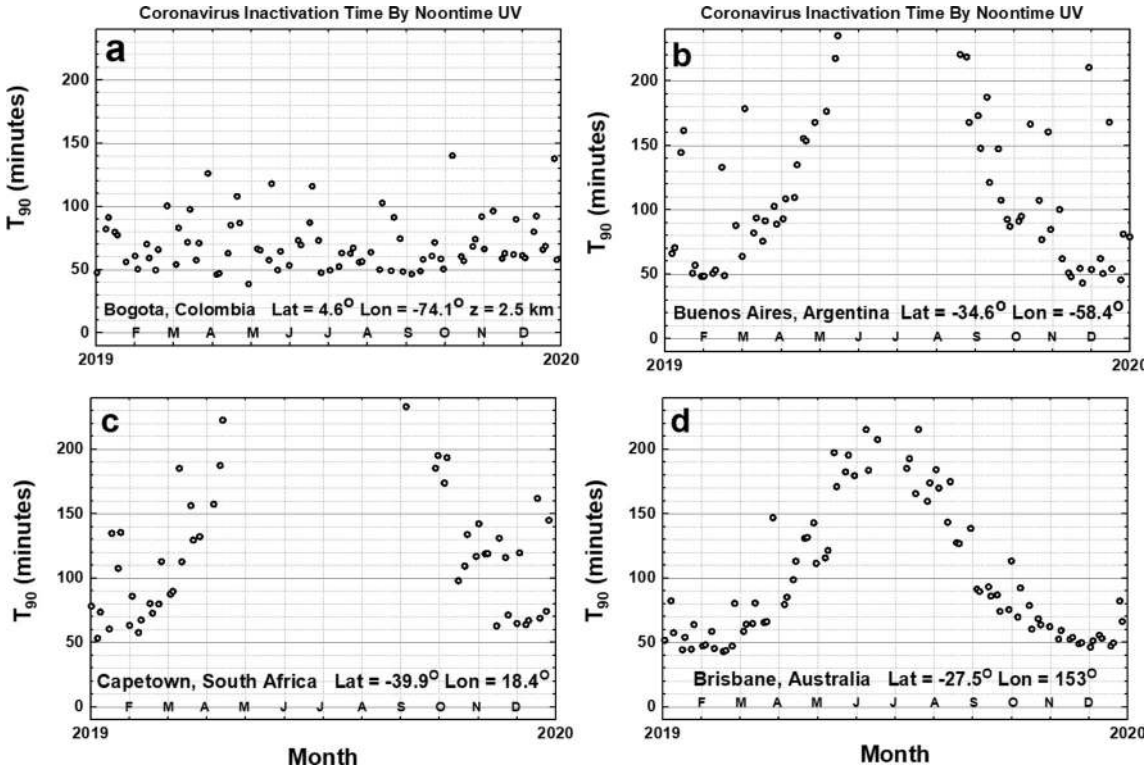

Fig. 7 Noontime T_{90} for an equatorial region city, Bogota, CO, and three cities in the Southern Hemisphere: Buenos Aires, AR; Cape Town, ZA; and Brisbane, AU using D_{90} = 40 J/m^2. For the calculated RS SARS CoV-2 D_{90} = 3.2 J/m^2, T_{90} in June would about 4 min for Bogota, in January 4 min Buenos Aires, Capetown, and Brisbane. Figures are truncated at 240 min

Estimates of variation with time of day for minimum <T_{90}>

The increase of T_{90} with SZA is shown in Fig. 2 for noontime irradiances. The same effect applies to other times of the day when θ increases relative to noon (Figs. 9 and 10). For solar times away from noon, the minimum of monthly averages $_{\text{Min}}$ <T_{90}> increases such that $_{\text{Min}}$ <T_{90}> 14:00> 70 min for all mid-latitude cities before 10:00 and after 14:00 h solar time. However, at 11:00 and 13:00 h, there are still a significant

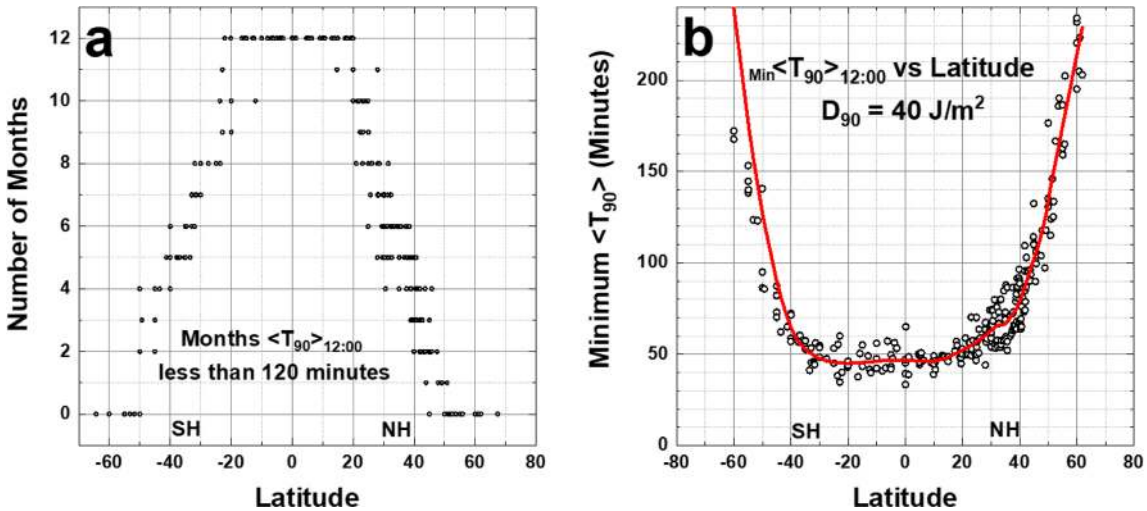

Fig. 8 **a** Number of months <T_{90}>$_{12:00} \leq$ 120 min from column 6 in Table s1. **b** Minimum $_{\text{Min}}$ <T_{90}>$_{12:00}$ vs. latitude from the data from column 5 in Table s1 as a function of latitude. The smoothed curve is a Loess(0.3) fit to the data. Loess(f) is locally weighted least squares fit to a fraction f of the data points, (Cleveland 1979, 1981). Figure is truncated at 240 min

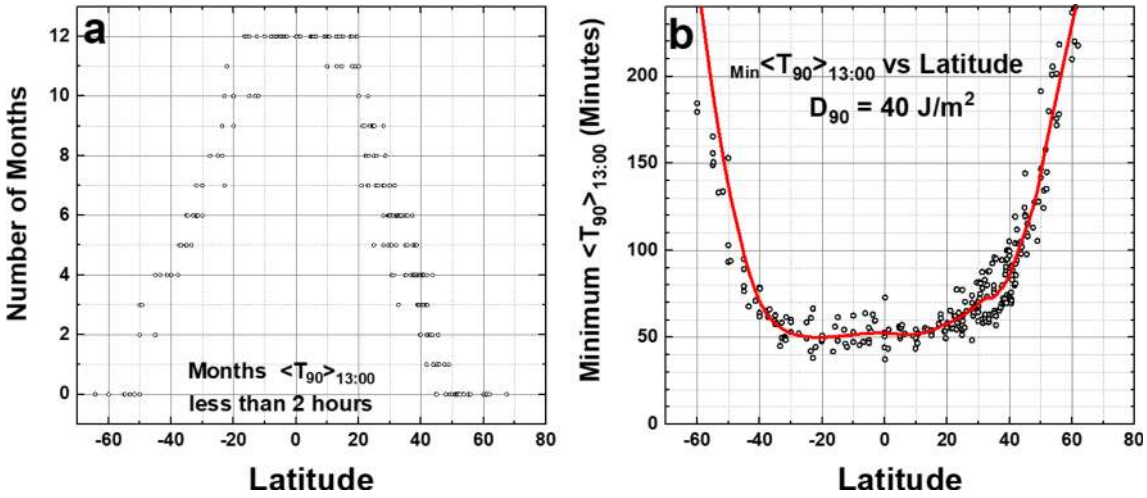

Fig. 9 **a** Number of months $<T_{90}>_{13:00} \leq 120$ min. **b** 13:00 h minimum $_{Min}<T_{90}>_{13:00}$ vs. latitude. The smoothed curve is a Loess(0.3) fit to the data. Figure is truncated at 240 min

number of mid-latitude sites with $_{Min}<T_{90}>_{13:00} < 75$ min and equatorial sites where $_{Min}<T_{90}>_{13:00} < 60$ min (Fig. 9a) for 2 or more months. Note that calculated $_{Min}<T_{90}>_{10:00} = {}_{Min}<T_{90}>_{14:00}$ and $_{Min}<T_{90}>_{11:00} = {}_{Min}<T_{90}>_{13:00}$.

Figure 10 compares the smoothed Loess (0.3) curves from Figs. 8b and 9b, plus a similar calculation for 14:00, showing the effect of time of day (12:00 to 14:00) on the minimum $_{Min}<T_{90}>_{Hour}$. The difference between $_{Min}<T_{90}>_{13:00}$ and $_{Min}<T_{90}>_{12:00}$ is from 5 to 10 min for sites between $\pm 30^{O}$ latitude extending to 25 to 30 min at 14:00.

Using the SARS CoV results from Figs. 2 and 10, it is possible to estimate the regions on the Earth where $_{Min}<T_{90}>_{Hour} < 50$ min and $_{Min}<T_{90}>_{Hour} < 65$ min and superimpose these criteria on color images from the DSCOVR/EPIC spectroradiometer to show the seasonal dependence driven by changes in the solar declination angle δ. Figure 11 shows solar illuminated Earth color images https://epic.gsfc.nasa.gov/ from sunrise to sunset obtained at the stated Greenwich Mean Time (GMT) for April 9, 2020 with the superimposed outer white circle representing the calculated 65-min $_{Min}<T_{90}>_{Hour}$ and the inner white circle the 50-min $_{Min}<T_{90}>_{Hour}$. Additional EPIC images are obtained approximately every 65 min (NH summer) to 108 min (NH winter) as the Earth rotates.

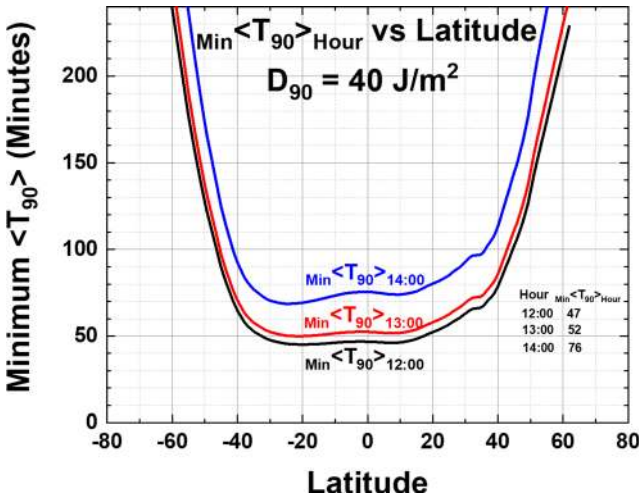

Fig. 10 Comparison of Loess $_{Min}<T_{90}>_{Hour}$ for 12:00, 13:00, and 14:00 h. The values at $\theta = 0^{O}$ are $_{Min}<T_{90}>_{Hour} = 47, 52, 76$ min at 12:00, 13:00, 14:00 h, respectively. Figure is truncated at 240 min

The images (Figs. 11 and 12) contain the subsolar point $\theta = 0^{O}$ with increasing θ radially in all directions away from the subsolar point. Since April 9 is 18 days after the March equinox, the subsolar point is about 7.6^{O} north of the equator. At 05:32:39 GMT, the clear-sky T_{90}(65 min) circle covers all of China and extends into southern Russia, Japan, and Korea. At 10:56:47 GMT, the outer circle covers southern Europe. Approximately 7 h later at 18:08:59 GMT, as the Earth rotates 15^{O} longitude per hour, EPIC is viewing North and South America where the 65-min $_{Min}<T_{90}>_{Hour}$ circle extends as far north as the border of Canada (about 48^{O} N) and as far south as the northern border of Chile (about 18^{O} S).

Figure 12 shows Earth images from days near the solstices in January and June 2019. The image from January 2, 2019 at 16:38:38 GMT shows the 65-min $_{Min}<T_{90}>_{Hour}$ circle extending to the middle of Africa and well south of Cape Town, South Africa. In contrast, on June 2, 2019 at 11:59:12 GMT, the subsolar point is near 23^{O} N and the 65-min $_{Min}<T_{90}>_{Hour}$ circle extends as far north as England and Germany. As the Earth rotates to later GMT, the 65-min $_{Min}<T_{90}>_{Hour}$ circle would contain all of South America and later, on the next calendar day, Australia and New Zealand.

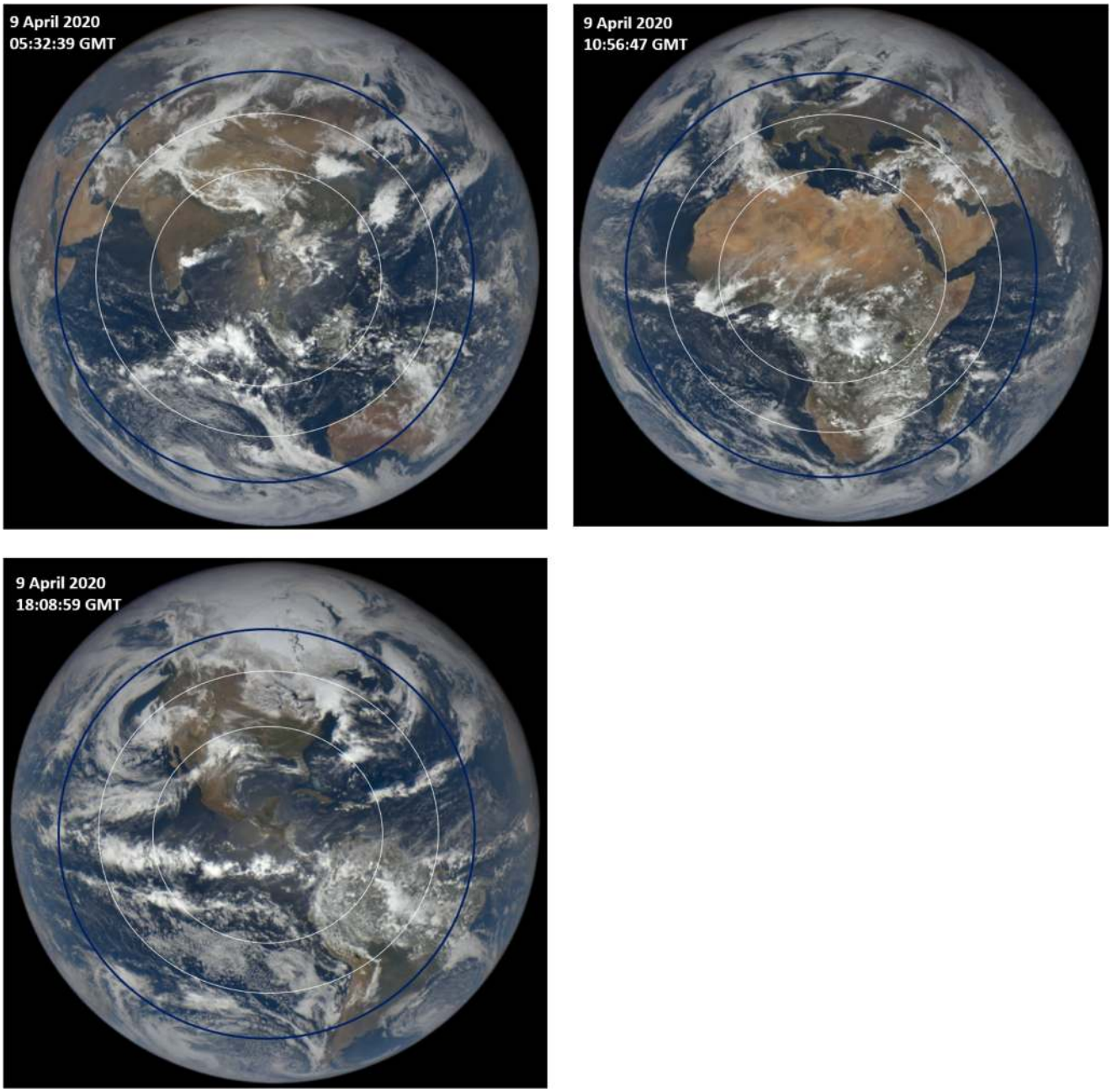

Fig. 11 Earth images from DSCOVR/EPIC for April 9, 2020 showing the superimposed outer circle (white) of clear-sky $_{Min}$ <T_{90}> less than 65 min and the inner circle (white) for $_{Min}$ <T_{90}> less than 50 min when D_{90} = 40 J/m^2. Sunrise is on the left (west) and sunset is on the right (east). The subsolar point is approximately in the center of the circle slightly offset by the small DSCOVR/EPIC orbital view angle. For the calculated RS SARS CoV-2 D_{90} = 3.2 J/m^2, a near-circle (dark-line) with solar zenith angle < 60^O centered on the subsolar point would have $_{Min}$ <T_{90}> less than 20 min

Since the EPIC images are synoptic, the longitudes are equivalent to local solar time of day (15^O/hour). For D_{90} = 40 J/m^2, the circles at their widest point are about 45^O or 3 h. This means that inactivation times are less than 65 min for Δt = 09:00 to 15:00 h for latitudes of the subsolar point in the equatorial region, ± 23.45^O. The longitudinal 65-min inactivation time-interval Δt decreases with increasing latitudinal distance away from the subsolar latitude δ, $\Delta t \approx 3\cos(\theta - \delta)$ hours for $|\theta - \delta| \leq 90^O$, where δ = solar declination angle. For the calculated RS SARS CoV-2 D_{90} = 3.2 J/m^2, longitudinal 20-min T_{90} inactivation time-interval $\Delta t \approx 4\cos(\theta - \delta)$ hours for $|\theta - \delta| \leq 90^O$.

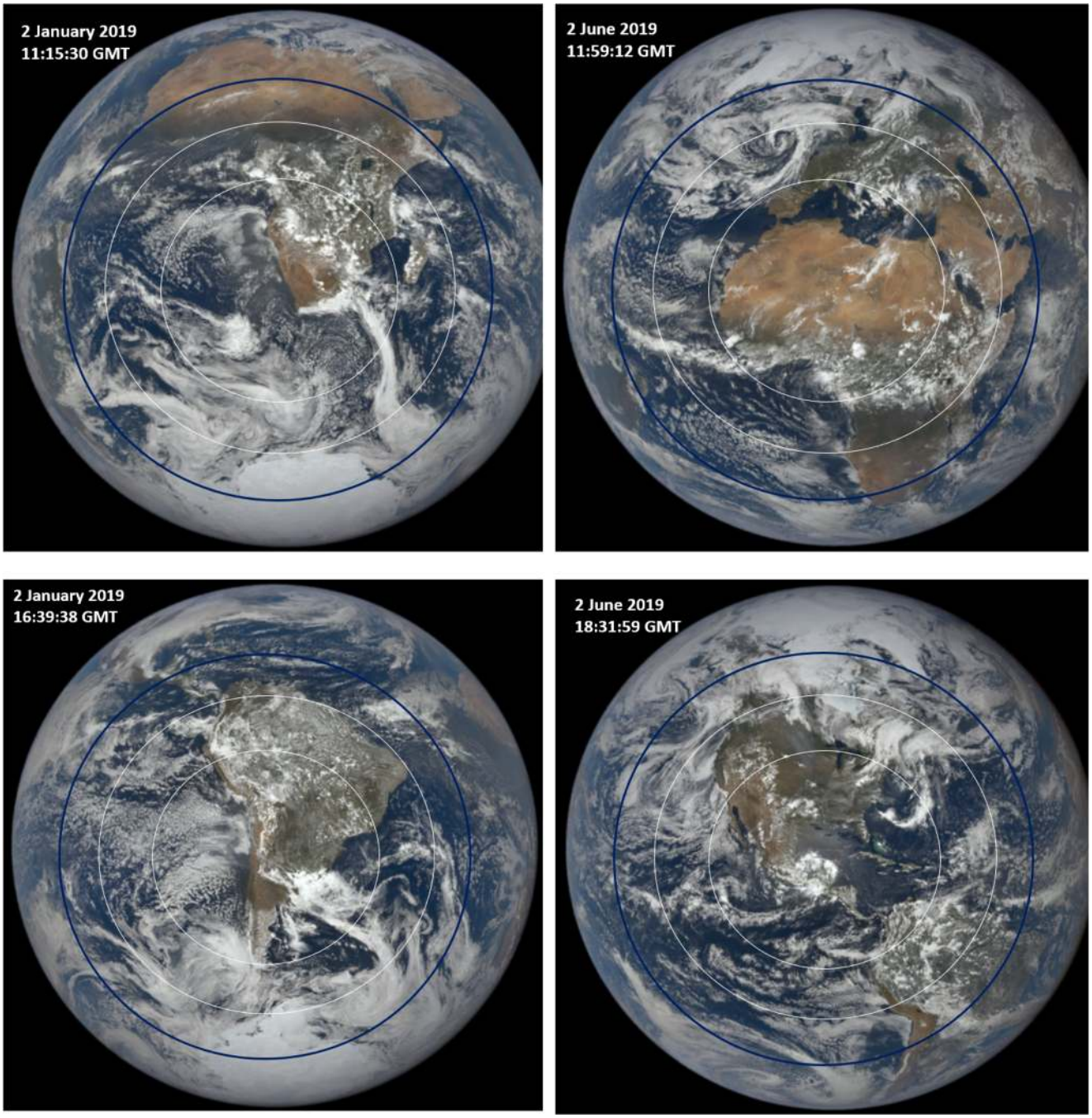

Fig. 12 Earth images from DSCOVR/EPIC for January 2, 2019 and June 2, 2019 showing the superimposed outer circle (white) of clear-sky $_{\text{Min}}\langle T_{90}\rangle$ less than 65 min and the inner circle (white) for $_{\text{Min}}\langle T_{90}\rangle$ less than 50 min when D_{90} = 40 J/m^2. Sunrise is on the left (west) and sunset is on the right (east). The subsolar point is approximately in the center of the circle slightly offset by the small DSCOVR/EPIC orbital view angle. For the calculated RS SARS CoV-2 D_{90} = 3.2 J/m^2, a near-circle (dark-line) with solar zenith angle < 60$^{\text{O}}$ centered on the subsolar point would have $_{\text{Min}}\langle T_{90}\rangle$ less than 20 min

Estimate of T_{90} for SARS-CoV-2 causing COVID-19

A recent study by Ratnesar-Shumate et al. (2020) performed laboratory studies of simulated June solstice solar UVB at 40$^{\text{O}}$ N inactivation of the SARS-CoV-2 virus that causes the current COVID-19 pandemic. RS compared the simulated UVB to solar amounts at the Earth's surface using the TUV radiative transfer model. Two basic experiments were run, one with droplets of virus in artificial saliva dried onto a stainless-steel mesh and the other using SARS-CoV-2 suspended in growth medium. As expected, it was found that inactivation times for virus suspended in a growth medium were significantly longer than for exposed virus on the steel mesh. Figures 13 and 14

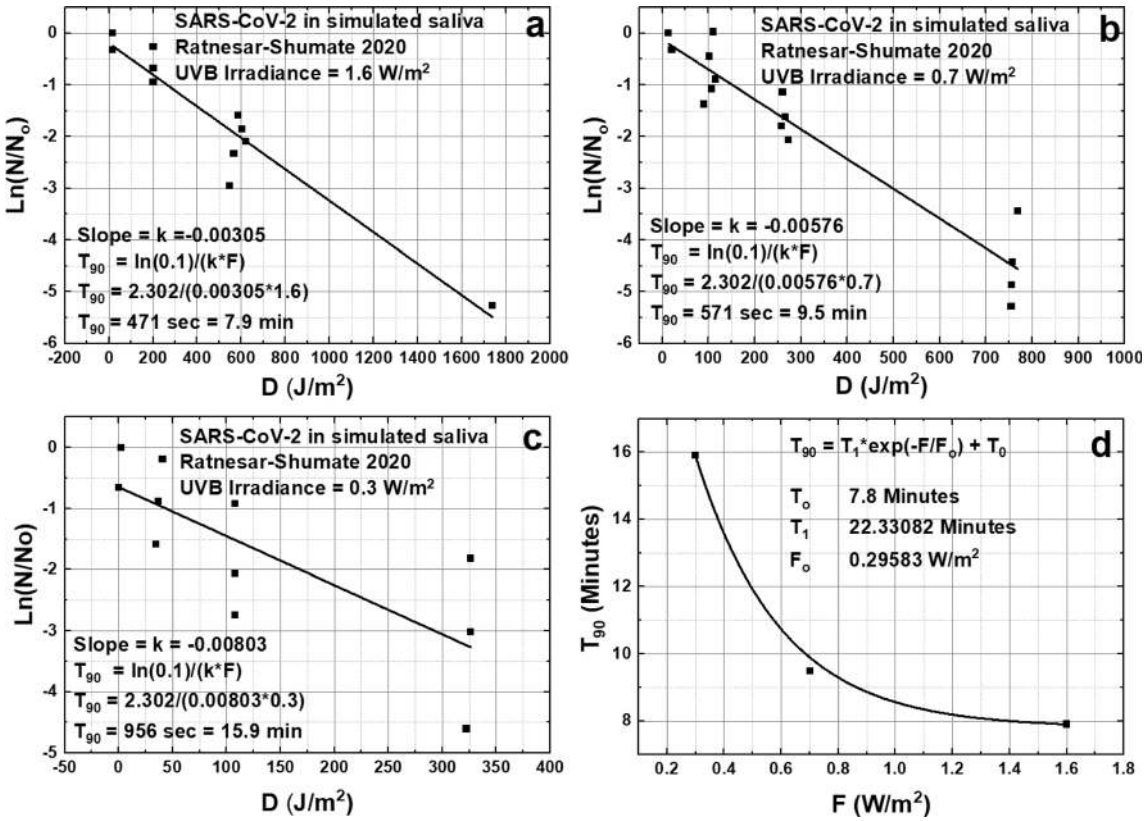

Fig. 13 Inactivation of the SARS-CoV-2 virus at three different irradiances of simulated solar UVB, panels **a**, **b**, and **c**, 1.6, 0.7, and 0.3 W/m^2 for the CoV-2 virus on a stainless-steel mesh surface based on the data from Fig. 4 of RS. Panel **d** is a summary of T_{90} from a, b, and c

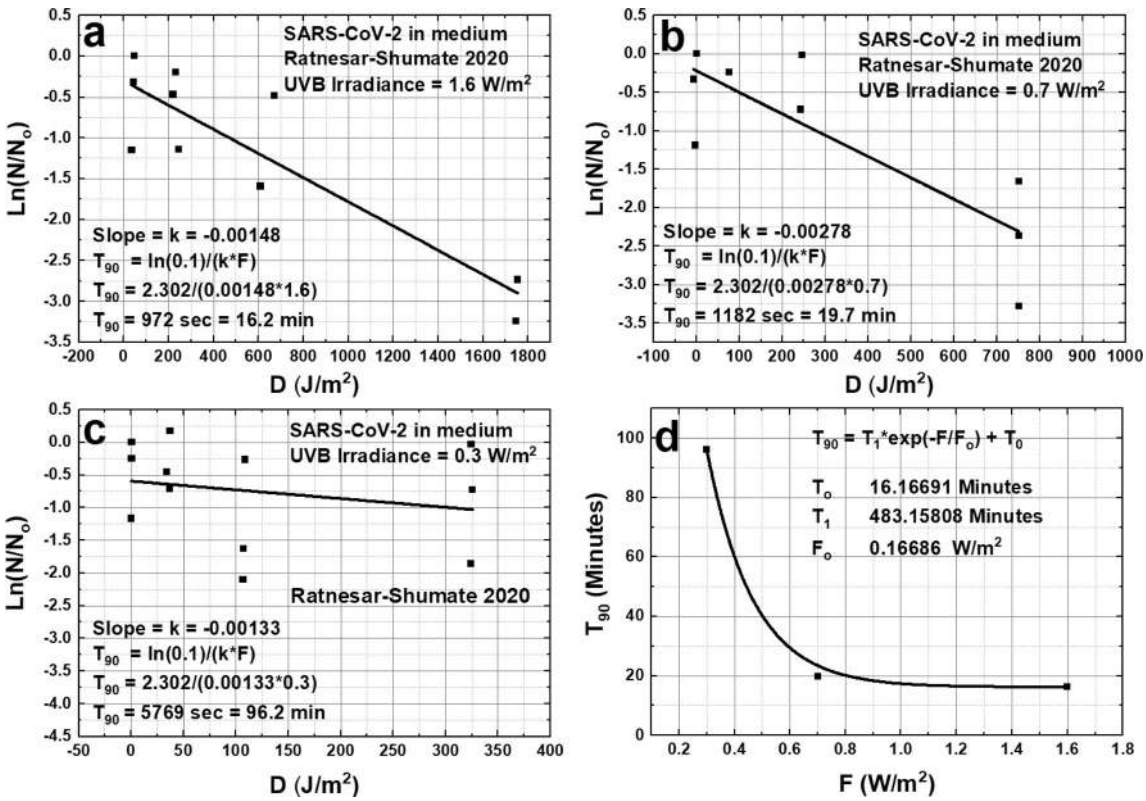

Fig. 14 Inactivation of the SARS-CoV-2 virus at three different irradiances of simulated solar UVB, panels **a**, **b**, and **c**, 1.6, 0.7, and 0.3 W/m^2 for CoV-2 virus suspended in a growth medium based on the data from Fig. 5 of RS. Panel **d** is a summary of T_{90} from a, b, and c

show RS data (electronic digitization of RS Figs. 4 and 5) in natural logarithmic form, that is, in terms of T_{90} on the assumption that the exponential decay model (Eq. 3) is applicable.

$$N/N_o = \exp(-kD) = \exp(-kPT) \quad (6)$$

$$T = -Ln(N/N_o)/(kP) \quad T_{90} = Ln(0.1)/(kP) \quad (7)$$

In Eqs 6 and 7, P (W/m^2) corresponds to Eq.1, T is the exposure time (seconds) and D is the UVB dose (J/m^2), where D = PT. In RS, P is not weighted with an action spectrum. The slope k (Figs. 13 and 14) is determined from a least squares linear fit to the survival fraction Ln(N/N$_o$) vs. the UVB dose D (J/m^2) for three different exposure rates. When P is small, the determination of k from Ln(N/N$_o$) is less certain.

In Fig. 13, the received UVB dose D is plotted against Ln(N/N$_o$) for three different UVB irradiances. Of these, the slope k for P = 0.3 W/m^2 has the largest uncertainty $k(0.3)$ = − 0.00803 ± 0.00221 compared to $k(1.6)$ = − 0.00305 ± 0.00031. The result is $T_{90}(1.6)$ = 7.9 min, $T_{90}(0.7)$ = 9.5 min and $T_{90}(0.3)$ = 15.9 min, all short inactivation times. Note that T_{999} values (99.9%) are four times T_{90}, which are still less than 1 h. These k estimates are slightly different than those in RS (6.8, 8.0, and 12.8 min, respectively), but do not significantly affect the current analysis and conclusions. The differences probably arise from different weighting of data points when RS's exposure times are almost zero (see RS's Figs. 4 and 5).

If it is assumed that the action spectrum $A(\lambda)$ applies, then the 254 nm UVC D_{90} equivalent is approximately DE$_{90}$ = 3.2 J/m^2 (Table 1) when using TUV calculations to approximate their result for 40^O N on June 21 at noon. Using the DE$_{90}$ value permits easy estimates of T_{90} for a wide range of geographic and atmospheric conditions. There are some differences between the simulated RS solar spectrum and the spectrum calculated here from TUV for different SZA in this study. The main difference is that the peak sensitivity shifts towards longer wavelengths (Fig. 2) as SZA or TCO$_3$ increases. Estimates of T_{90} for SARS CoV-2 are not significantly affected by the choice of $A(\lambda)$, since the value of D_{90} was adjusted to match the simulated UVB amounts in RS. RS measurements made in simulated sunlight give an error estimate of ± 10% (their Fig. 5). Estimating DE$_{90}$ requires combining the two independent errors giving an error of 22%, or DE$_{90}$ = 3.2 ± 0.7 J/m^2.

When the same exposures are applied to the virus in a growth medium the RS-based results are shown in Fig. 14. $T_{90}(1.6)$ = 16.2 min and $T_{90}(0.7)$ = 19.7 min compared to RS's values of 14.3 and 17.6. As above, using the action spectrum $A(\lambda)$ gives a 254 nm UVC D_{90} equivalent of approximately 6.5 ± 1.4 J/m^2 (Table 1).

A recent analysis for the SARS CoV-2 inactivation times (Sagripanti and Lytle 2020) obtains an estimate for D_{37} = 3.0 J/m2, which translates to D_{90} = 3 ln(0.1)/ln(0.37) = 6.9 J/m^2, larger than the estimate for D_{90} = 3.2 J/m^2 given above. The methods for obtaining D_{90} are entirely different. The method used here relies on finding a value of 254 nm D_{90} that yields approximately the same inactivation time, 6.8 min, as RS finds for midday during the summer solstice at 40^O N latitude using the same TUV radiative transfer code. Sagripanti and Lytle (2020) infer their value from laboratory measurements of viruses with a similar genomic structure and "the fact that UVC sensitivities of viruses depends proportionally on genome size, especially with single-stranded RNA or DNA." Most of the measurements they reference were made with viruses in a liquid medium and should be compared to the value obtained from RS data, using the radiative transfer method, of 6.5 J/m^2 for viruses in a growth medium.

The values of T_{90} estimated by Sagripanti and Lytle (2020) are 3 to 4 times larger than estimated here. Part of the difference arises from their estimate of D_{90} being 2.15 times larger. The remainder must come from the estimate of noontime solar flux entering into $\int F(\lambda)\, A(\lambda) d\,\lambda$ in Eq. 1. They use an approximation to the noontime solar flux based on 35% of the daily fluence occurring during a 2-h period surrounding solar noon. "Thus, 35% of the total daily UVB fluence divided by 120-min yields the noontime UVB flux(in J m^{-2} min^{-1})." The noontime F(λ) in Eq 1 is calculated using the SZA and local atmospheric parameters for each site estimated from OMI data, which may differ from the 35% estimate.

If RS's smaller values for T_{90} are used instead of the values in Figs. 13 and 14, then the UVC equivalent would be smaller than D_{90} = 3.2 J/m^2 estimated here. The value D_{90} = 3.2 J/m^2 is approximately 12.5 times smaller than the UVC D_{90} = 40 J/m^2 for the SARS CoV virus used in the previous sections leading to T_{90} of about 4 min at the equator and about 5 min at 40^O N during the summer solstice (Fig. 15b). The main conclusion that SARS CoV-2 virus is quickly inactivated by UVB in sunlight remains unchanged. For estimating day-to-day inactivation times, the exact T_{90} numbers for SARS CoV-2 virus are unimportant on any given day because of the larger T_{90} variability caused by significant atmospheric transmission changes even on days that appear relatively clear of clouds and aerosols.

The RS measurements show that T_{90} for SARS CoV-2 on a surface is smaller than in a growth medium, which is similar to the results for the airborne MHV virus D_{90} = 6.6 J/m^2 and the same virus in liquid, D_{90} = 95 J/m^2, with the value in liquid (Table 1) much greater than the value in air.

Figure 16 shows the inactivation times for SARS CoV-2 virus on surfaces by solar UVB for three different times of the day when D_{90} = 3.2 J/m^2, which is the approximate equivalent RS's laboratory simulated solar UVB. The results show minimum inactivation times $_{Min}$ <T_{90}>

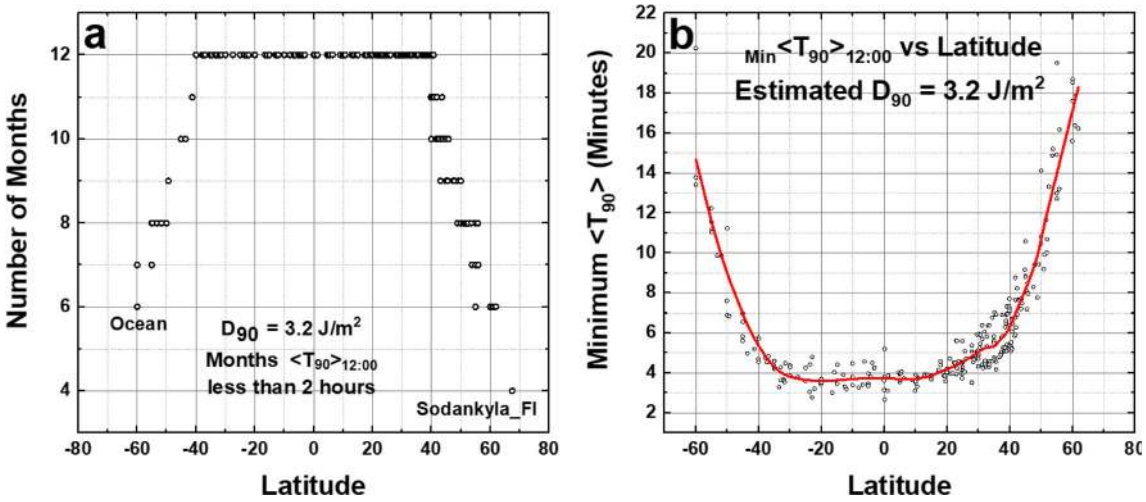

Fig. 15 **a** Number of months $_{\text{Min}}\langle T_{90}\rangle_{12:00} \leq 120$ min (column 8 Table s1). **b** Minimum $_{\text{Min}}\langle T_{90}\rangle_{12:00}$ vs. latitude as a function of latitude (column 7 Table s1). The smoothed curve is a Loess(0.3) fit to the data. For the estimated RS SARS CoV-2 D_{90} = 3.2 J/m^2, T_{90} values at all latitudes − 60^{O} to 60^{O} are less than 18 min and the minimum values at the equator are T_{90} = 4 min

increasing as |LST–12:00| increases, but always less than 1 h. For high latitude sites considered (latitude ≥ 60^{O}) during the winter months T_{90} inactivation times are much longer than 2 h and, on many days, no inactivation is possible. For example, Sodankylä, Finland has only 4 months during which the inactivation time T_{90} < 2 h (Fig. 15a).

As the time of day increases to 16:00 LST a peculiar SZA effect occurs because of the spherical geometry. The minimum SZA for near solstice conditions shifts to higher latitudes near 40^{O} north and south, causing $_{\text{Min}}\langle T_{90}\rangle_{14:00}$ to be smaller at 35^{O} S and 35^{O} N than it is near the equator. Note that these are annual minimum T_{90} that includes both summer solstices in their respective hemispheres giving rise to two minima.

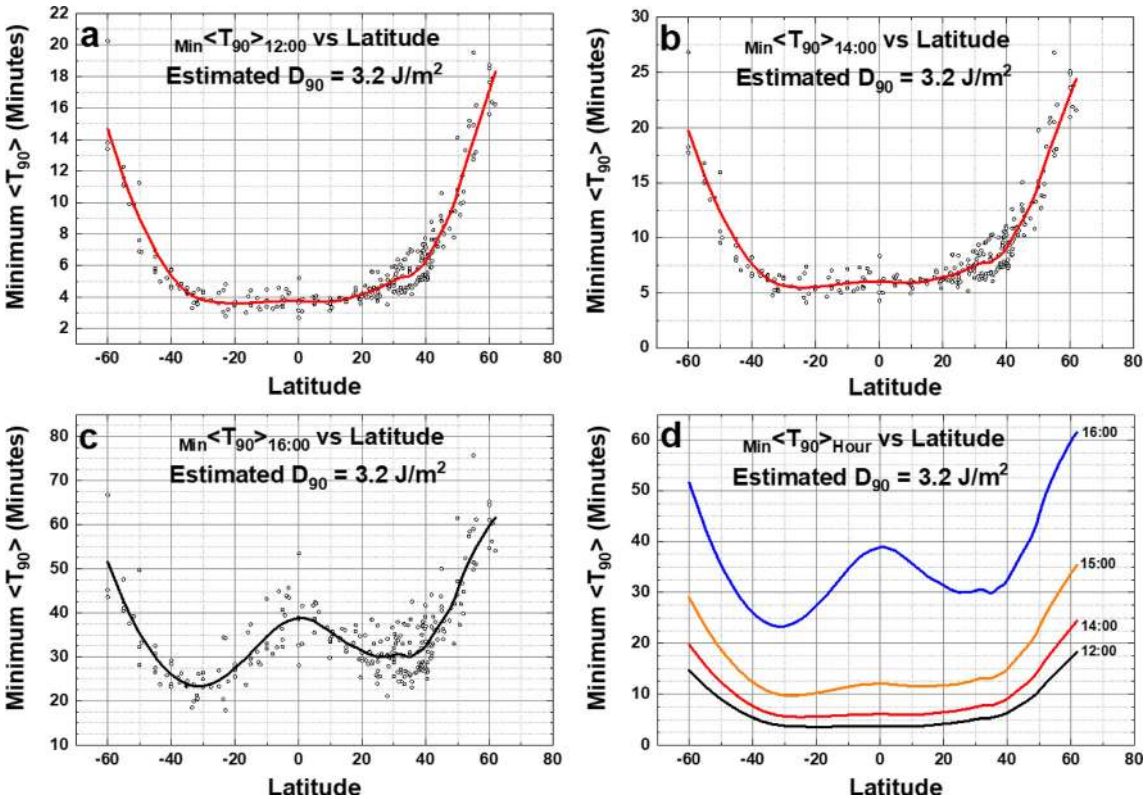

Fig. 16 Estimated inactivation times for SARS Cov-2 virus dried on surfaces as a function of latitude at 12:00, 14:00, and 16:00 local solar time for the calculated RS D_{90} = 3.2 J/m^2. **a** 12:00, **b** 14:00, **c** 16:00, **d** compare four different hours

Summary and discussion

A study of coronavirus inactivation times by UV solar irradiation is presented for two classes of experimental laboratory data. First, are those measurements made at 254 nm and extrapolated to wavelength longer than 290 nm using an action spectrum $A(\lambda)$ (Lytle and Sagripanti 2005), and second, are the measurements made in simulated sunlight (Ratnesar-Shumate et al. 2020) that do not require the use of an action spectrum. For the RS case, $A(\lambda)$ is used to estimate the value of 254 nm D_{90} that gives approximately the same T_{90} derived by RS for a June solstice at 40° N (254 nm $D_{90} = 3.2 \pm 0.7$ J/m^2 for dried virus droplets on a steel mesh surface and 6.5 ± 1.4 J/m^2 for viruses in a growth medium).

A fast calculation method, which closely approximates TUV radiative transfer results for clear and cloudy scenes, has been used for calculating 90% inactivation times T_{90} for SARS CoV and SARS CoV-2 viruses in a realistic atmosphere when exposed to sunlight based on 90% inactivation doses D_{90} at 254 nm. The method uses OMI satellite data for cloud transmission, ozone, and aerosol absorption over a wide range of latitudes, longitudes, and day of the year. For SARS CoV, a nominal value $D_{90} = 40$ J/m^2 is used for 90% inactivation at 254 nm combined with the assumed applicable virus inactivation action spectrum $A(\lambda)$ provided by Lytle and Sagripanti (2005). The results are used to calculate midday amounts of UVB from sunlight that can deactivate coronaviruses on horizontal surfaces by 90% in moderate amounts of time, $T_{90} < 90$ min at mid-latitudes, for low latitudes $T_{90} < 60$ min and for equatorial region sites $T_{90} < 50$ min. The SARS CoV $D_{90} = 40$ J/m^2 model suggests that outdoor horizontal surfaces that have been unoccupied for at least 90 min and exposed to clear-sky midday levels of UVB sunlight are likely to have coronaviruses 90% inactivated during the Spring through Autumn months for mid- and low-latitude sites where $T_{90} \leq 90$ min, and all year for equatorial sites. T_{90} results are also presented for different times of the day over a wide range of latitudes and SZA. Estimates are given for the number of months in each year that a given location has $T_{90} < 2$ h (Figs. 9, 10, 15, 16, and Table s1).

Inactivation by sunlight to undetectable levels of virus will take much longer, perhaps 2 to 3 times longer based on laboratory inactivation by UVC. For aerosolized particles carrying the SARS CoV virus, $D_{90} = 7.11$ J/m^2 (Walker and Ko (2007), the value for the T_{90} value is reduced by a factor of 40/7.11 = 5.63. Of course, viruses deposited late in the day may persist overnight with inactivation delayed until the following day. The presence of common light to moderate cloud cover, LER < 0.3, increases the inactivation time as shown by the scatter in Figs. 5, 6, and 7.

For the recent Ratnesar-Shumate et al. (2020) laboratory results, the calculated equivalent 254 nm SARS CoV-2 $D_{90} = 3.2 \pm 0.7$ J/m^2. Calculated $T_{90} < 7$ min at mid-latitudes, while for the equatorial region sites $T_{90} < 4$ min, the reduction in T_{90} is a factor of 12.5 compared to using $D_{90} = 40$ J/m^2. For the calculated RS SARS CoV-2 $D_{90} = 3.2$ J/m^2, minimum inactivation times are less than 20 min for local solar times from 10:00 to 14:00 h and less than 60 min solar zenith angels $\theta < 60^{O}$ from the subsolar latitude for 08:00 to 16:00 h. For those surfaces that are near direct sunlight, but not in direct sunlight, there is ample diffuse UVB sunlight to inactivate SARS CoV-2 coronaviruses with about 70% more exposure, or less than 2 h for mid-latitudes and for equatorial sites in less than 90 min. At other times of the day between 11:00 and 13:00 local solar time, there are still many mid- and low-latitude sites with sufficient sunlight so that $_{\text{Min}}\langle T_{90}\rangle_{13:00} \leq 90$ min. By 14:00 h, there are very few sites with $_{\text{Min}}\langle T_{90}\rangle_{14:00} \leq 90$ min. During the summer solstices the $_{\text{Min}}\langle T_{90}\rangle_{12:00} \leq 65$ min circles cover mid-latitude cities in both hemispheres. Cities at high latitudes greater than 60^{O} do not have periods where the inactivation times are less than 2 h. Unoccupied midday surfaces will become relatively virus free in short periods from Spring to Autumn. While sunlight will inactivate the SARS CoV-2 virus responsible for COVID-19, the midday UVB 90% inactivation time, 7 to 20 min, is too slow to protect against transmission between people outdoors in crowds.

Acknowledgments The authors would like to thank and acknowledge the support of the DSCOVR project and the OMI science team for the OMI satellite project for making OMI data freely available.

Authors' contributions Jay Herman is responsible for all of the calculations, figures, and large portions of the text. Bryan Biegel is responsible for motivating this study, significant portions of the text, and careful review of the entire paper. Liang Huang is responsible for supplying the OMI satellite data properly filtered for bad pixels and the row anomaly

Funding This research is supported by the DSCOVR/EPIC NASA project under UMBC task 00011511

Data availability All data used in this study are available in stated public archives, listed references, or included explicitly in the study.

Compliance with ethical standards

Conflict of interest The authors have no conflicts or of interest or competing interests

Code availability The radiative transfer code TUV is publicly available as described in the references. Graphics and analysis use OriginLab Origin Pro software

References

Anderson DJ, Gergen MF, Smathers E, Sexton DJ, Chen LF, Weber DJ, Rutala WA (2013) Decontamination of targeted pathogens from patient rooms using an automated ultraviolet-C-emitting device. Infect Cont Hosp Ep 34(5):466–471. https://doi.org/10.1086/670215

Bedell K, Buchaklian A, Perlman S (2016) Efficacy of an automated multiple emitter whole-room ultraviolet-C disinfection system against coronaviruses MHV and MERS-CoV. Infect Cont Hosp Ep 37(5):598–599. https://doi.org/10.1017/ice2015348

Cleveland WS (1979) Robust locally weighted regression and smoothing scatter plots. J Am Stat Assoc 74:829–836. https://doi.org/10.1080/01621459197910481038

Cleveland WS (1981) A program for smoothing scatterplots by robust locally weighted regression. Am Stat 35(1):54. https://doi.org/10.2307/2683591

Darnell MER, Subbarao K, Feinstone SM, Taylor DR (2004) Inactivation of the coronavirus that induces severe acute respiratory syndrome, SARS-CoV. J Virol Methods 121:85–91. https://doi.org/10.1016/jjviromet200406006

Duan SM, Zhao XS, Wen RF, Huang JJ, Pi GH, Zhang HJ, Bi SL, Ruan L, Dong XP (2003) Stability of SARS coronavirus in human specimens and environment and its sensitivity to heating and environment and UV irradiation. Biomed Environ Sci 16:246–255

Eisenstark A (1987) Mutagenic and lethal effects of near-ultraviolet radiation (290–400 nm) on bacteria and phage. Environ Mol Mutagen 10:317–337. https://doi.org/10.1002/em2850100311

Herman J (2010) Use of an improved radiation amplification factor to estimate the effect of total ozone changes on action spectrum weighted irradiances and an instrument response function. J Geophys Res 115. https://doi.org/10.1029/2010JD014317

Herman JR, Celarier EA (1997) Earth surface reflectivity climatology at 340 nm to 380 nm from TOMS data. J Geophys Res 102:28,003–28,011. https://doi.org/10.1029/97JD02074

Herman JR, Labow G, Hsu NC, Larko D (2009) Changes in cloud and aerosol cover (1980-2006) from reflectivity time series using seawifs, N7-TOMS, EP-TOMS, SBUV-2, and OMI radiance data. J Geophys Res 114:D01201. https://doi.org/10.1029/2007JD009508

Herman J, Huang L, McPeters R, Ziemke J, Cede A, Blank K (2018) Synoptic ozone, cloud reflectivity, and erythemal irradiance from sunrise to sunset for the whole earth as viewed by the DSCOVR spacecraft from the earth–sun Lagrange 1 orbit. Atmos Meas Tech 11:177–194. https://doi.org/10.5194/amt-11-177-2018

Herman J, Cede A, Huang L, Ziemke J, Kowalewski M, Blank K (2020) Global Distribution and 14-year changes in erythemal irradiance, UV atmospheric transmission, and total column ozone 2005–2018 estimated from OMI and EPIC observations. Atmos Chem Phys. https://doi.org/10.5194/acp-2019-793

Heßling M, Hönes K, Vatter P, Lingenfelder C (2020) Ultraviolet irradiation doses for coronavirus inactivation - review and analysis of coronavirus photoinactivation studies. GMS Hyg Infect Control 15:Doc08. https://doi.org/10.3205/dgkh000343

Kampf G, Todt D, Pfaender S, Steinmann E (2020) Persistence of coronaviruses on inanimate surfaces and their inactivation with biocidal agents. J Hosp Infect 104:246–251. https://doi.org/10.1016/jjhin202001022

Kariwa H, Fujii N, Takashima I (2004) Inactivation of SARS coronavirus by means of povidone-iodine, physical conditions, and chemical reagents. Jpn J Vet Res 52:105–52,112. https://doi.org/10.1159/000089211

Kowalski W (2009) Ultraviolet germicidal irradiation handbook, UVGI for air and surface disinfection. Springer, Heidelberg. https://doi.org/10.1007/978-3-642-01999-9

Kowalski W, Bahnfleth W, Hernandez M (2009) A genomic model for predicting the ultraviolet susceptibility of viruses. IUVA News 11:15–24

Kowalski W, Walsh T, Petraitis V (2020a) COVID-19 coronavirus ultraviolet susceptibility, purplesun technical report. https://doi.org/10.13140/RG222280322566

Kowalski WJ, Bahnfleth WP, Raguse M, Moeller R (2020b) The cluster model of ultraviolet disinfection explains tailing kinetics. J Appl Microbiol 128(4):1003–1014. https://doi.org/10.1111/jam14527

Lakkala K, Kujanpää J, Brogniez C, Henriot N, Arola A, Aun M, Auriol F, Bais AF, Bernhard G, De Bock V, Catalfamo M, Deroo C, Diémoz H, Egli L, Forestier J-B, Fountoulakis I, Garcia RD, Gröbner J, Hassinen S, Heikkilä A, Henderson S, Hülsen G, Johnsen B, Kalakoski N, Karanikolas A, Karppinen T, Lamy K, León-Luis SF, Lindfors AV, Metzger J-M, Minvielle F, Muskatel HB, Portafaix T, Redondas A, Sanchez R, Siani AM, Svendby T, Tamminen J (2020) Validation of TROPOMI surface UV radiation product. Atmos Meas Tech Discuss. https://doi.org/10.5194/amt-2020-121 in review

Levelt PF, Joiner J, Tamminen J, Veefkind JP, Bhartia PK, Stein Zweers DC, Duncan BN, Streets DG, Eskes H, van der A R, McLinden C, Fioletov V, Carn S, de Laat J, DeLand M, Marchenko S, McPeters R, Ziemke J, Fu D, Liu X, Pickering K, Apituley A, González AG, Arola A, Boersma F, Miller CC, Chance K, de Graaf M, Hakkarainen J, Hassinen S, Ialongo I, Kleipool Q, Krotkov N, Li C, Lamsal L, Newman P, Nowlan C, Suleiman R, Tilstra LG, Torres O, Wang H, Wargan K (2018) The ozone monitoring instrument: overview of 14 years in space. Atmos Chem Phys 18:5699–5745. https://doi.org/10.5194/acp-18-5699-2018

Liu Y, Cai Y, Zhang X (2003) Induction of caspase-dependent apoptosis in cultured rat oligodendrocytes by murine coronavirus is mediated during cell entry and does not require virus replication. J Virol 77:11952–11963. https://doi.org/10.1128/JVI772211952-119632003

Lytle CD, Sagripanti J-L (2005) Predicted Inactivation of viruses of relevance to biodefense by solar radiation. J Virol:14244–14252. https://doi.org/10.1128/JVI792214244-142522005

Madronich S (1993) The atmosphere and UV-B radiation at ground level. In: Björn LO, Young AR (eds) Environmental UV Photobiology. Plenum, New York, pp 1–39

Madronich S (1995) The radiation equation. Nature 377:682

Michalsky JJ, Kiedron PW (2008) Comparison of UV-RSS spectral measurements and TUV model runs for clear skies for the May 2003 ARM aerosol intensive observation period. Atmos Chem Phys 8:1813–1821. https://doi.org/10.5194/acp-8-1813-2008

Mok J, Krotkov NA, Torres O, Jethva H, Li Z, Kim J, Koo J-H, Go S, Irie H, Labow G, Eck TF, Holben BN, Herman J, Loughman RP, Spinei E, Lee SS, Khatri P, Campanelli M (2018) Comparisons of spectral aerosol single scattering albedo in Seoul, South Korea. Atmos Meas Tech 11:2295–2311. https://doi.org/10.5194/amt-11-2295-2018

Nelson KL, Boehm AB, Davies-Colley RJ, Dodd MC, Kohn T, Linden KG, Liu Y, Maraccini PA, McNeill K, Mitch WA, Nguyen TH, Parker KM, Rodriguez RA, Sassoubre LM, Silverman AI, Wigginton KR, Zepp RG (2018) Sunlight-mediated inactivation of health-relevant microorganisms in water: a review of mechanisms

and modeling approaches. Environ Sci Process Impacts 20:1089–1122. https://doi.org/10.1039/c8em00047f

Ratnesar-Shumate S, Williams G, Green B, Krause M, Holland B, Wood S, Bohannon J, Boydston J, Freeburger D, Hooper I, Beck K, Yeager J, Altamura LA, Biryukov J, Yolitz J, Schuit M, Wahl V, Hevey M, Dabisch P (2020) Simulated sunlight rapidly inactivates SARS-CoV-2 on surfaces. J Infect Dis:jiaa274. https://doi.org/10.1093/infdis/jiaa274

Sagripanti JL, Lytle CD (2020) Estimated inactivation of coronaviruses by solar radiation with special reference to COVID-19. Photochem Photobiol 96(4):731–737. https://doi.org/10.1111/php.13293

Schenkeveld VME, Jaross G, Marchenko S, Haffner D, Kleipool QL, Rozemeijer NC, Veefkind JP, Levelt PF (2017) In-flight performance of the ozone monitoring instrument. Atmos Meas Tech 10:1957–1986. https://doi.org/10.5194/amt-10-1957-2017

Torres O, Tanskanen A, Veihelmann B, Ahn C, Braak R, Bhartia PK, Veefkind P, Levelt P (2007) Aerosols and surface UV products from ozone monitoring instrument observations: an overview. J Geophys Res 112:D24S47. https://doi.org/10.1029/2007JD008809

Walker CM, Ko G (2007) Effect of ultraviolet germicidal irradiation on viral aerosols. Environ Sci Technol 41:5460–5465. https://doi.org/10.1021/es070056u

Weiss M, Horzinek MC (1986) Resistance of Berne virus to physical and chemical treatment. Vet Microbiol 11:41–49. https://doi.org/10.1016/0378-1135(86)90005-2